Journal of
Materials Chemistry C

PAPER

View Article Online
View Journal

Cite this: DOI: 10.1039/c6tc00542j

Twofold photoswitching of NIR fluorescence and EPR based on the PMI–N–HABI for optical nanoimaging of electrospun polymer nanowires†

Wen-Liang Gong,‡ Zu-Jing Xiong,‡ Bo Xin,‡ Hong Yin,‡ Jia-Shun Duan,‡ Jie Yan,‡ Tao Chen,‡ Qiong-Xin Hua,‡ Bin Hu,‡ Zhen-Li Huang*‡ and Ming-Qiang Zhu*‡

Received 5th February 2016,
Accepted 1st March 2016

DOI: 10.1039/c6tc00542j

www.rsc.org/MaterialsC

In this article, we report the design and synthesis of a fluorescent molecular switch based on perylenemonoimide–hexaarylbiimidazole dyad (PMI–N–HABI), which exhibits not only photoswitchable near-infrared (NIR) fluorescence but also photoswitchable electron paramagnetic resonance (EPR) resulting from photo-induced twin radicals. The emission of PMI–N–HABI varies with different polarities of solvents due to the D–π–A molecular architecture, displaying strong NIR emission (715 nm) in methylene chloride with fluorescence quantum yield as high as 0.29. The photo-induced cleavage of the C–N bond between the two imidazole groups produces twin radicals efficiently upon UV irradiation and the colored species recovered to the initial state spontaneously by the collision of the two intramolecular TPIRs in a few seconds, with decay (or fluorescence recovery) half-life time ($\tau_{1/2}$) of 1.3 s in toluene at 297 K. The radical nature of the colored species is verified by EPR measurements. The emission of the perylenemonoimide could be reversibly quenched by the photo-induced radicals through the Forster resonance energy transfer (FRET) mechanism. The fluorescence-switching dye is applied to the optical nanoimaging of polymer nanowires prepared using the typical electrospinning method. The average diameter of about 160 nm is in accordance with the scan electron microscopic (SEM) images. Compared with the traditional SEM technique, we provide a convenient alternative to SEM with practical imaging resolution for polymer nanostructures.

Introduction

Fluorescence molecular switches have attracted much attention because they possess much higher sensitivity upon light irradiation than molecular photochromism.[1–3] The applications of photochromic materials have ranged from optical data storage,[4] sensors,[5] and photochromic lenses[6] to more recent applications such as light-emitting organic memory,[7] super-resolution imaging,[8] optical transistors,[9] encoding light information,[10] photochromic nanoflasks,[11] and optobioelectronic applications.[12] Of them, fluorescence switching is more promising in all-optical switches and transistors as well as super-resolution imaging.[13] A great deal of efforts have been made to design novel fluorescence switching mechanisms and develop new fluorescence molecular switches from blue to red emission during the past ten years.[14–16]

The design and synthesis of fluorescence photoswitches are generally established by connecting a dyad with a photochromic unit. Among the large family of organic dyes, perylene dyes (including perylene bisimide, perylene monoimide, terylene bisimide and so on) are always the first choice for organic chemists on many occasions because of their superior optical properties with high molecular absorptivity, fluorescence quantum yield of close to 1, high photostability and easy functionalization for specific applications.[17] More recently, fluorescence photoswitches based on perylene dyes with DTE, spiropyran and other photochromes have found applications in devices such as non-destructive readout memory devices[18,19] and logic gates.[20] While the emission wavelengths of these reported systems are in the visible light (less than 700 nm) range except for terylene dyes, which face the problem of complicated synthesizing work, poor solubility and relative small stoke shift values.[21] Alternatively, the emission of perylene dyes could be tuned by the introduction of electron-donating groups in conjugation with the perylene core, in which the D–A structure was established taking the advantage of the electron with-drawing nature of imide moieties.[22]

Hexaarylbiimidazoles (HABIs) have been extensively investigated as a novel photochromic molecule because of their thermal spontaneous fading from colorful radical recombination.[23–28] The colorless HABI dimer can be homolytically cleaved (photodissociation) to form a pair of colored 2, 4, 5-triphenylimidazoyl twin radicals followed by the back reaction (association) to form

Wuhan National Laboratory for Optoelectronics, College of Optical and Electronic Information, Huazhong University of Science and Technology, Wuhan, Hubei 430074, China. E-mail: mqzhu@hust.edu.cn, leo@hust.edu.cn

† Electronic supplementary information (ESI) available. See DOI: 10.1039/c6tc00542j

‡ These authors contributed equally.

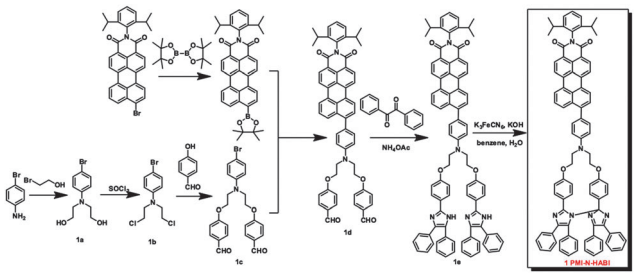

Scheme 1 The synthetic procedures of PMI–N–HABI.

the original dimers, which is induced thermally. The advantages of HABIs as photochromic molecules include photo-induced paramagnetic activity and long wavelength absorption, which are beneficial to the switching of long wavelength emission.[23,24] Previous reports on fluorescence HABIs demonstrate that the emission wavelength (from blue to red), photo-induced absorption wavelength and fluorescence recovery rate are tuned depending on different molecular architectures. Due to the increased research interest and attention regarding fluorescent photochromes for a wide variety of applications, we are dedicated to develop a more fluorescent photoswitchable system, in particular, with NIR emission. Here we design and synthesise a fluorescent HABI-based photochrome, in which a highly fluorescent perylenemonoimide (PMI) derivative is connected to HABI in a non-conjugated fashion (Scheme 1). It is discovered that the fluorescence molecular switch PMI–N–HABI exhibits featured photoswitchable NIR emission and photo-induced paramagnetic activity, which sparks a promising prospective in super-resolution imaging.

Experimental section

Chemicals

The preparation and characterization of the precursors for PMI–N–HABI are reported in detail in the ESI.† All solvents, reagents and chemicals are commercially available and used as supplied, unless otherwise stated. Chloroform is dried over calcium hydride under stirring overnight followed by distillation under normal pressure. THF and toluene are dried using a sodium wire–benzophenone system and distillation. The other solvent used in this work, like cyclohexane, chlorobenzene, ethyl acetate, methylene chloride, acetonitrile, are distilled before use in optical measurements. DMSO was stirred with CaH_2 overnight and then distilled under reduced pressure. PMI–N–HABI is synthesized following the procedures given below.

Synthesis of PMI–N–HABI (1)

Into a 250 ml two-neck flask, **1e** (0.2 g, 0.16 mmol) was dispersed in 50 ml benzene. This solution was vigorously stirred and covered from daylight by an aluminum foil. Consequently, an aqueous solution (50 ml) of $K_3Fe(CN)_6$ (2.63 g, 8 mmol) and KOH (0.90 g, 16 mmol) was added dropwise in 20 min. The reaction was detected by a TLC plate until the starting material was totally converted. After the completion of the reaction, the organic layer was collected, washed with brine (3 × 50 ml), dried over $MgSO_4$ and filtered. The resulting solution was then evaporated under a reduced pressure for purification by column chromatography on Al_2O_3 (200–300) using DCM and ethyl acetate as the eluent (500–20 ml). 140 mg of black solid was obtained, with a yield of 70%. ^{1}H NMR δ_H (CD_2Cl_2, 600 MHz): 8.60 (t, J = 6 Hz, 2H), 8.50 (m, 4H), 8.18 (d, J = 6 Hz, 1H), 7.60 (m, 4H), 7.48 (m, 6H), 7.20–7.40 (m, 17H), 7.14 (t, J = 18 Hz, 2H), 7.10 (m, 4H), 6.88 (d, J = 6 Hz, 2H), 6.73 (d, J = 6 Hz, 2H), 6.57 (d, J = 6 Hz, 2H), 4.47 (t, J = 6 Hz, 2H), 4.33 (t, J = 6 Hz, 2H), 3.75 (d, J = 6 Hz, 2H), 3.61 (d, J = 6 Hz, 2H), 2.80 (m, 2H), 1.19 (d, J = 6 Hz, 12H); ^{13}C NMR δ_C (DMSO-d, 600 MHz): 160.55, 145.87, 135.46, 131.75, 130.87, 129.52, 129.43, 129.08, 129.01, 128.80, 128.69, 128.61, 127.70, 127.51, 127.04, 126.86, 122.07, 115.08, 111.44, 29.07, 27.19, 24.18, 19.76; MALDI-TOF m/z: calculated 1246.5146 (100.0%), 1247.5179 (93.0%), 1248.5213 (42.8%), 1249.5246 (12.9%), 1250.5280 (2.9%), 1247.5116 (2.2%), 1248.5149 (2.1%); found 1247.2260, 1248.3764; elemental analysis: required C, 82.80; H, 5.33; N, 6.74; O, 5.13; found C, 82.75; H, 5.36; N, 6.71; O, 5.10.

EPR

The EPR measurements were performed on a Bruker EPR A300 machine (X band).

Electrospinning of the polymer

The nanowires were prepared by a electrospinning method using PVP (M_n = 1 300 000) in a mixture of solvents (DMF and ethanol) with a weight ratio of 1 : 7 : 2. PMI–N–HABI (5 mg) was dissolved into this polymer solution (10 ml), which was used directly for electrospinning. During the electrospinning process, the voltage was controlled at 20 kV and the consuming speed of the polymer solution was 10 ml in half an hour.

Optical nanoimaging

The optical setup for imaging was based on a home-built microscope setup consisted of an Olympus IX71 inverted optical microscope, a 100×/NA1.49 oil immersion TIRF objective (UAPON 100XOTIRF, Olympus), three solid-state lasers (405, 473, and 561 nm, all from CNILaser, China), and an AndoriXon 897 EMCCD camera. During super-resolution imaging, two electronic shutters (UNIBLITZ VS14, Vincent Associates) were used to control the duration of laser irradiance, and a dichroic mirror (Di01-R488/561, Semrock) and a long pass filter (BLP01-561R-25, Semrock) were used to separate the collected fluorescence from the scattering laser and impurity fluorescence. The Image J plugins written in Java was used to analyze the images.

Results and discussion

We proposed the design and synthesis of PMI–N–HABI, in which the two triphenylimidazole groups are locked by the special structure of a dioxyethylene amine bridge. In a solution of 2-bromoethanol (excess amount), 4-bromoaniline and sodium bicarbonate were added under stirring at 57 °C for 2 days to yield the corresponding products, **1a**. Then using thionyl chloride, **1a** was converted to 4-bromo-*N*,*N*-bis (2-chloroethyl)

aniline (**1b**) in dry CH_2Cl_2. In a solution of DMF with potassium carbonate, **1b** reacted with *p*-hydroxybenzaldehyde at 100 °C for 2 days, yielding **1c** in high yield (95%). PMI (*N*-(2,5-di-*tert*-butylphenyl)perylene-3,4-dicaboximde) and 9-Br-PMI (9-bromo-*N*-(l-hexylheptyl)perylene-3,4-dicaboxirnide) were prepared according to the work reported by Leonhard Feiler *et al.*[29] The synthesis of PMI-borate was performed via typical procedures using $Pd(dppf)Cl_2$ as the catalyst, potassium acetate as the base and 1,4-dioxane as the solvent under a N_2 atmosphere for 12 h, with a yield of 74%. **1c** and PMI-borate were then reacted in toluene with potassium carbonate and $Pd(PPh_3)_4$ (catalyst) under a N_2 atmosphere to yield **1d**. **1d**, benzil, ammonium acetate and a catalytic amount of acetic acid were dispersed in $CHCl_3$, stirred and heated to 110 °C in a sealed tube for 2 days to yield **1e**. Then **1e** was dispersed in degassed toluene and to this solution an aqueous solution of K_3FeCN_6/KOH was added in darkness. The product was purified by column chromatography on Al_2O_3 (200–300) to yield PMI–N–HABI as black-purple solid (70%). The detailed synthetic procedures could be found in the ESI.†

Optical properties of PMI–N–HABI

We investigate the optical absorption and emission of PMI–N–HABI in different solvents. The results are shown in Table 1. Basically, the maximum absorption wavelength red-shift increases with the increase in solvent polarity, from 516 nm (cyclohexane) to 548 nm (DMSO). In comparison, the emission wavelength of PMI–N–HABI is 591 nm in cyclohexane while the value becomes 719 nm in THF, which is a pronounced red-shift. The apparent maximum Stokes shift attains 175 nm in methylene chloride (DCM). The fluorescence quantum yield of PMI–N–HABI in polar solvents is much lower than that in nonpolar solvents.

As we can see from the molecular structure of PMI–N–HABI, the imide part of PMI–N–HABI works as a strong electron-withdrawing group and the aniline part as an electron-donating group. In this way, a "D–π–A" structure is established. PMI–N–HABI exhibits typical intramolecular charge transfer (ICT) properties in organic solvents (Fig. 1a and b). The maximum absorption wavelength $\lambda_{abs,max}$ was calculated to be 516 nm in the non-polar solvent, cyclohexane (CH) (Fig. 1a). This value increases gradually with the change of the solvent from a weak polar solvent (toluene, $\lambda_{abs,max}$ = 528 nm) to a strong polar solvent (DMSO, 548 nm). Meanwhile, the $\lambda_{em,max}$ also exhibits similar trends (Fig. 1b), 591 nm in CH and 715 nm in DCM. In strong polar solvents like acetonitrile (ACN) and DMSO, the emission is so weak that the $\lambda_{em,max}$ could not be calculated clearly. However, the fluorescence quantum yield (Φ_F) decreases greatly with the change of the solvent from a non-polar solvent (CH, 0.63) to a strong polar solvent (ACN, 3.6×10^{-3}). These are typical characteristics for the molecules with ICT properties.

Table 1 Optical properties of PMI–N–HABI in organic solvents

Solvent	$\lambda_{abs,max}$	$\lambda_{em,max}$	FLQY	Stokes shift (nm)
Cyclohexane	516	591	0.63	75
Toluene	528	627	0.53	99
Chlorobenzene	540	678	0.39	138
Ethyl acetate	528	714	0.20	86
Methylene chloride	540	715	0.29	175
THF	533	719	0.13	86
Ethanol	543	—	0.011	—
Acetonitrile	534	—	3.6×10^{-3}	—
DMSO	548	—	2.7×10^{-3}	—

Notes: "— means the value not be determined; the relative fluorescence quantum yield is calculated using RhB as the standard (QY = 0.7, in ethanol).

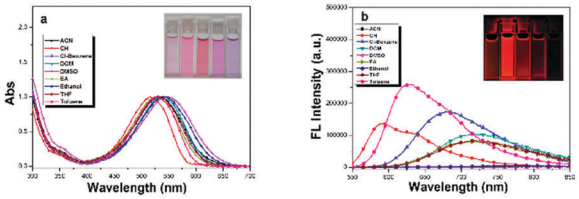

Fig. 1 Optical properties of PMI–N–HABI: (a) UV-vis and (b) FL spectra of PMI–N–HABI in various organic solvents. Inset photos: PMI–N–HABI in cyclohexane, toluene, chlorobenzene, methylene chloride and dimethyl sulfoxide under daylight and UV (365 nm), respectively.

The fluorescence properties of PMI–N–HABI, which are highly dependent on the polarity of the solvents, could be explained by the intramolecular-charge transfer (ICT) due to its strong "D–π–A" structures. The increased conjugation length leads to the strong red-shift of the emission in different solvents, which has also been reported in similar structures like triphenylamine (TPA), piperazine substituted perylene bisimides (PBI)[30,31] and perylene monoimide (PMI).[32,33]

DFT calculation of PMI–N–HABI

In order to further understand the optical properties of PMI–N–HABI, we performed the electron density distribution calculation of PMI–N–HABI using the model of B3LYP exchange–correlation functional and a 6-31G* basis, and the corresponding results are presented in Fig. 2. The electron cloud is homogenously distributed in the PMI and aromatic amine moieties in the ground state (HOMO); while in the LUMO or the excited state, the electrons are "transferred" towards the imide part of PMI and nearly no electron distribution remains in the aromatic amine moiety. These electron distribution differences between the HOMO and the LUMO definitely support the deduction of ICT characteristics of PMI–N–HABI. It is clear that the HABI

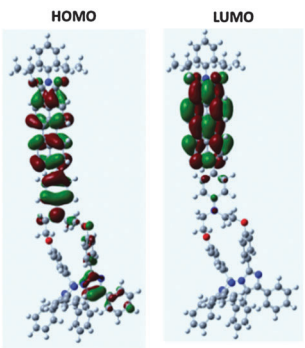

Fig. 2 HOMO and LUMO of PMI–N–HABI calculated by DFT calculation.

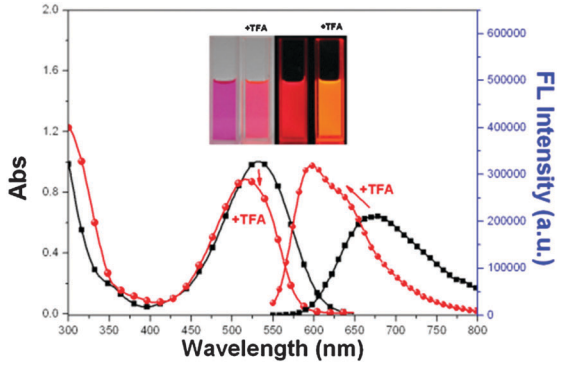

Fig. 3 FL and UV-vis spectra of PMI–N–HABI in $CHCl_3$ (black line) and $CHCl_3$/TFA = 9 : 1 (red line) with concentration equals to 1.2×10^{-5} mol L^{-1}; inset photos of PMI–N–HABI in $CHCl_3$ with/without adding TFA in daylight and UV 365 nm.

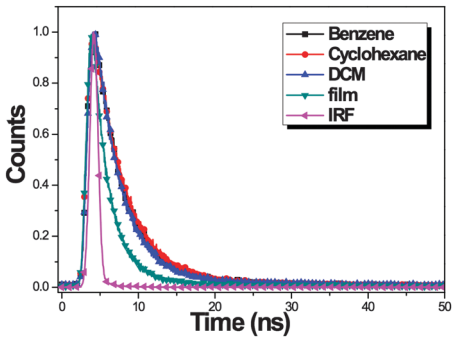

Fig. 4 Fluorescence lifetime spectra of PMI–N–HABI in benzene (630 nm), cyclohexane (590 nm), DCM (715 nm) and film (750 nm); the excitation source is equipped with a 532 nm laser.

moiety shares no conjugation with those of PMI moieties, thus it would not affect the fluorescence properties, or in other words, the PMI–aniline moiety is fully responsible for the fluorescence properties of PMI–N–HABI.

Protonation of PMI–N–HABI

We investigated the protonation effect on fluorescence of PMI–N–HABI due to the amino group. It is found the change in absorption and emission spectra of PMI–N–HABI in $CHCl_3$ solution after the addition of TFA by accident and the corresponding optical spectra are shown in Fig. 3. Generally, $\lambda_{em,max}$ and $\lambda_{abs,max}$ of PMI–N–HABI blue shifted from 672 to 592 nm with a clear shoulder peak at around 630 nm and 532–516 nm, respectively. Meanwhile, due to the H^+ sensitive characteristics of HABIs, we exclude the spectra changes of PMI–N–HABI from the HABI moieties by performing the same experiments using **1d** instead of PMI–N–HABI. A similar phenomenon has also been observed when we used the mediatory product **1d**, suggesting that the 9–4′-amine-benzene substituted PMI is responsible for the optical properties (Fig. S1, ESI†). We suppose that the H^+ ionization from TFA could neutralize the amine part of PMI–N–HABI, thus the electron resonance through the π-conjugation from aniline to the perylenemonoimide core was inhibited and both the $\lambda_{em,max}$ and $\lambda_{abs,max}$ of PMI–N–HABI in $CHCl_3$ are blue-shifted as a result. On the other hand, TFA could reduce the π–π aggregation between perylene cores, which causes a slight increment in the emission intensity.[34–37] In other words, the TFA experiments indicate the "D–π–A" characteristics of PMI–N–HABI in another way.

Fluorescence lifetime of PMI–N–HABI in organic solvents and films

The fluorescence lifetimes of PMI–N–HABI in solution (benzene, cyclohexane and DCM) and solid states are measured and the corresponding data are presented in Fig. 4. Although the $\lambda_{em,max}$ values of PMI–N–HABI in different solvents vary greatly, the fluorescence lifetime of PMI–N–HABI in solution exhibits very little change with the increase in polarity, from cyclohexane, benzene to DCM (see Fig. 4). The fluorescence lifetime in benzene ($\tau_{benzene}$) is calculated to be 3.94 ns (χ^2 = 1.713, Fig. S2a and b, ESI†). However, the lifetime in a solid film is much different from those in solutions and the experimental data were fitted to be two lifetimes, which are 2.0 and 3.3 ns (χ^2 = 1.229, Fig. S2c and d, ESI†). The strong π–π stacking interactions of perylene (and its derivatives) have been widely investigated. The fluorescence lifetime of PMI–N–HABI in the dilute solution generally shares one lifetime with similar values, which indicates that the fluorescence process in various polarity media are the same. While the strong π–π stacking interaction of PMI–N–HABI in the film might induce the H-aggregation between two molecules. Thus the $\lambda_{em,max}$ of PMI–N–HABI in the film highly red shifted to 750 nm with quenched emissions, indicating the non-radiation process domains.

Photochromism and fluorescence switching of PMI–N–HABI

The photochromism and fluorescence switching properties of PMI–N–HABI in the solid state have been investigated in the thin film and the corresponding UV-vis and FL spectra are presented in Fig. 5 with different UV irradiation times. The film was prepared by dissolving PMI–N–HABI in distilled DCM, and this solution was added dropwise onto a clean quartz in darkness. After the solvent was slowly evaporated, the film was further dried under vacuum at 80 °C for 6 h. In the solid state, a broad absorption at around 700–900 nm appears, which might be due to the strong π–π stacking between PMI–N–HABI molecules. Under UV irradiation, the absorption at around 600–800 nm increases and a clear new peak appears at around 390 nm. When we used optical density changes to analyze these characteristics, the absorption characteristics of the new species formed upon UV irradiation become much clearer (Fig. 5a inset). The absorption changes at 390 nm are nearly the same with those of $C_8H_{17}O$-TPIRs (Fig. S3, ESI†). The broad absorption peak at around 610 nm of PMI-N-2O-TPIRs, generated from the radical–radical interaction, separated into two peaks (514 and 660 nm) compared with that of $C_8H_{17}O$-TPIRs. It is reasonable note that these spectra changes might be caused by the strong aggregation of perylene cores, which facilitate the photo-induced electron transfer from TPIR moieties to the perylene core.

At the same time, we also measured the changes of the FL spectra upon UV irradiation (Fig. 5b). The $\lambda_{em,max}$ of PMI–N–HABI

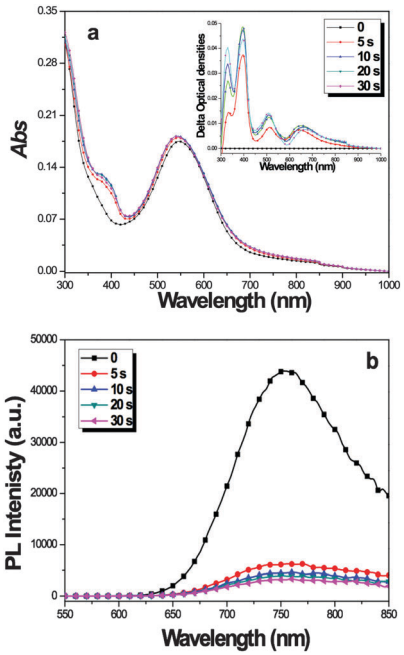

Fig. 5 (a), UV-vis and (b), fluorescence spectra of PMI–N–HABI in the film under irradiation of 302 nm with the time varying from 0, 5, 10, 20 to 30 s; the inset in (a) is the changes of optical absorption with different irradiation time.

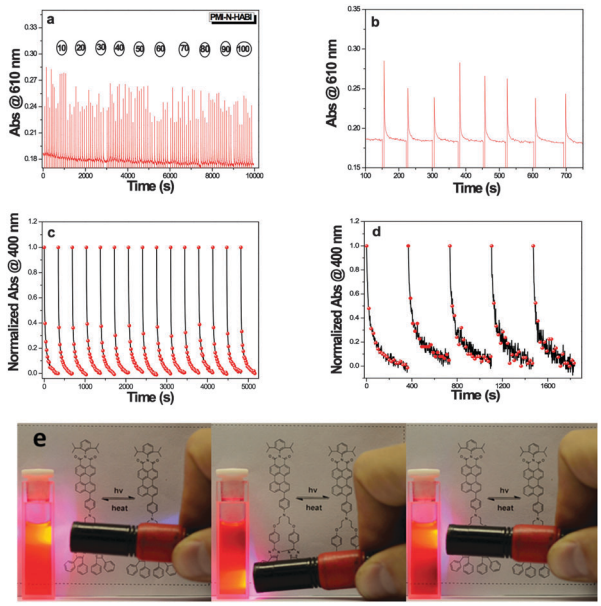

Fig. 6 Fading kinetics of PMI–N–HABI. (a) In toluene for more than 100 cycles. (b) Expansion of the area from 100 to 750 s. (c) In PMMA film for more than 15 cycles. (d) In PS film. (e) Photos of PMI–N–HABI in toluene upon excitation by an UV laser pen. The concentration of PMI–N–HABI in toluene solution is 8.1×10^{-5} mol L^{-1} (297 K).

is found to be 750 nm, which might be due to the strong aggregation in the solid state. The emission intensity decreases sharply in 5 s of irradiation and remains nearly unchanged after 30 s of irradiation. Generally, according to our previous results,[38–40] we attributed these absorption changes to the photochromism of PMI–N–HABI, which are generated from the photo-induced C–N cleavage in the HABI moiety. Thus the fluorescence of PMI–N–HABI is quenched through the FRET process from the PMI to the TPIRs under UV irradiation.

Reversible photochromic and simultaneous fading kinetics of PMI–N–HABI in solution

In order to investigate the fading kinetics of PMI–N–HABI in solution, we perform the real-time monitoring measurements of optical density at 610 nm (Fig. 6). PMI–N–HABI is first dissolved in toluene with the concentration controlled to 5×10^{-5} mol L^{-1} and then degassed with N_2 to exclude the remaining O_2 for 0.5 h. UV-vis spectroscopy is widely considered to be a powerful equipment for the investigation of photochromism phenomena. Thus we use an UV LED to irradiate the solution (3 s) and record the optical density changes at 610 nm upon alternating 3 s of UV LED irradiation in every 50 s of interval. The coloration and de-coloration processes could be performed for more than 100 times and no clear photobleaching of PMI–N–HABI was observed (Fig. 6a). After UV irradiation, PMI–N–HABI is converted to PMI-N-2TPIRs with an increased absorption at 610 nm. As the UV source ceases, PMI-N-2TPIRs recombined spontaneously to form PMI–N–HABI with the absorbance recovered to the initial values (Fig. 6b). The half-life time of PMI-N-TPIR for this whole process was calculated to be 1.3 s at 24 °C, and the photochromic phenomenon is also presented in Fig. 6e. Meanwhile, the molecular design of PMI–N–HABI with improved fading kinetics compared to C_8H_{17}-O-HABI is also directly proved by a movie (see the ESI† movie).

The photochromic and fatigue resistance properties were further tested in a solid substrate and a polymer film. Here we chose two of the most popular polymers: polystyrene (PS) and PMMA. Before sample preparation, 5 g of polymer (PMMA and/or PS) were dissolved in 50 ml distilled DCM and stirred overnight. To this polymer solution (1 mL), 1 mg PMI–N–HABI was added and this solution was used in spin-coating at 1000 rad s^{-1} for 1 min. The resulting films were then dried in darkness to get rid of the remaining solvents. Similarly, we monitored the absorbance decay kinetics at 400 nm with time after UV irradiation for 3 s. The increases of the absorbance could be attributed to the photo-induced transformation of PMI–N–HABI to PMI-N-2TPIRs and the gradual decrease represents the simultaneous reverse fading process. In comparison with that in solution, the fading kinetics of PMI–N–HABI in the polymer film is rather slow and the complete de-coloration takes about 300 s with the half-life time as long as 40 s (Fig. 6c and d). These characters have been attributed to the slower molecular motion because the radicals are trapped in the polymer matrix, thus the collision efficiencies of TPIRs are decreased. In both PMMA and PS films, PMI–N–HABI exhibits excellent fatigue resistance for more 15 cycles.

EPR measurement of PMI–N–HABI in solution

The mechanism of photo-induced homogeneous cleavage of C–N between the two imidazole rings in PMI–N–HABI is also investigated by EPR measurements. In principle, HABIs show

no EPR signals in both solutions until suitably treated by, *e.g.*, light or heat to form the corresponding radicals. As we have claimed before,[38–40] the oxygen-substituted HABI is responsible for the photochromic, fluorescence and electron paramagnetic switching of PMI–N–HABI. The EPR signal of PMI–N–HABI was obtained by the irradiation of the solution of PMI–N–HABI (benzene) under a 405 nm laser during the experiments. As references, we also performed similar measurements with HABI and $C_8H_{17}O$-HABI in the same way. The EPR spectrum of TPIR (formed from HABI) is similar in structure but different in the G values from that of $C_8H_{17}O$-TPIR (formed from $C_8H_{17}O$-HABI) (see Fig. S4, ESI†). This could be attributed to the difference in their molecular structures while the EPR spectrum of PMI-N-2TPIR is nearly the same as that of $C_8H_{17}O$-TPIR, which suggests that the oxygen-substituted TPIRs are responsible for the photoswitchable EPR in PMI–N–HABI (see Fig. S4, ESI†).

In order to investigate the kinetic process of photo-induced cleavage of HABIs in forming radicals, we performed the EPR measurements of $C_8H_{17}O$-HABI in benzene at 293 K (Fig. S5, ESI†) by using a 405 nm laser for different times for comparison. Without irradiation, the $C_8H_{17}O$-HABI solution exhibits poor EPR signals. After 5 s of irradiation, a strong EPR signal at around 3510 G was observed and the signal kept on increasing with the accumulated irradiation time (Fig. S5, inset plot, ESI†). These characters are in accordance with the UV-vis spectra changes in solutions. Since the time consumed for every EPR spectrum is around the level of seconds in our lab currently, we could hardly perform the same experiments for PMI–N–HABI due to the relatively fast fading kinetics of the radicals of PMI–N–HABI as we have proved above (Fig. 6a). We believe the difference of the fading kinetics between $C_8H_{17}O$-HABI and PMI–N–HABI was the main reason. The kinetics speed of $C_8H_{17}O$-TPIRs and $C_8H_{17}O$-HABI in collision is rather slow (at 293 K), so we obtained a nice plot of increasing EPR signals with the accumulated irradiation time. While for PMI–N–HABI, the half-life time was calculated to be 1.3 s at 298 K, which was too short to collect the data with the accumulated irradiation time. In order to prove this, we perform the experiments at a low temperature (100 K) to slow down the recombination speed of PMI-N-OTPIRs. As shown in Fig. 7a, the EPR spectra of PMI–N–HABI exhibit increasing signals with the accumulated irradiation time (Fig. 7a inset).

Meanwhile, the fading kinetics of PMI–N–HABI after irradiation was also real time investigated by EPR measurements at 293 K and 100 K. The experiments were performed *via* continuous scanning to collect the EPR signals after 10 s of irradiation using a 405 nm laser. The time interval between two scans was about 2 s. As we can see from Fig. 7b, the EPR signals measured at 293 K decreased by more than 50% at scan **2** (black line) compared to scan **1** (red line) and the EPR completely disappeared after 10 scans while at a low temperature of 100 K (Fig. S6, ESI†), the EPR spectra were nearly unchanged after 9 scans (about 18 min in total). These data indicate that the photo-induced twin radicals PMI-N-2TPRs are thermally-sensitive. At a low temperature of 100 K, the dynamics of radicals is much slower than that at room temperature.

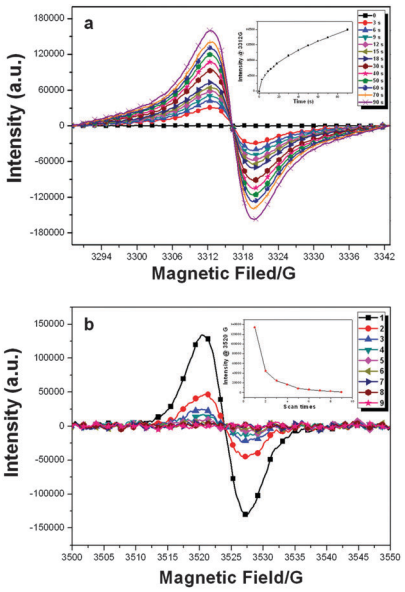

Fig. 7 (a) EPR spectra of PMI–N–HABI in benzene solution at 100 K upon different irradiation times of a 405 nm laser (100 mW); the inset is the plot of magnetic field intensity at 3312 G with irradiation time. (b) The EPR fading kinetics of PMI–N–HABI in benzene solution at room temperature (298 K) after 10 s of irradiation by a 405 nm laser (the scan interval: 2 s); the inset is the plot of magnetic field intensity at 3520 G with different scans. The concentration of PMI–N–HABI is 10^{-3} M.

Super-resolution imaging of nanowires prepared by electrospinning

The microstructures of the synthesized nanowires are characterized by SEM and fluorescence microscopy equipped with two lasers: 405 and 561 nm. During the super-resolution imaging experiments, a 561 nm laser was used as an excitation source and a 405 nm laser as UV light to induce photochromism of the HABI moiety. The fluorescence recovers upon ceasing illumination of the 405 nm laser for a while (about 2 min) and this has been repeated for many cycles during the fluorescence imaging processes. The preparation of the nanowires by electrospinning and the corresponding super-resolution imaging process of the nanowires are illustrated in Scheme 2.

The wide-field, fluorescence, SEM and super-resolution images are presented in Fig. 8. Generally, it is difficult to obtain the accurate size of nanowires whose diameters are below 200 nm in the bright field (Fig. 8a) and conventional fluorescence (Fig. 8b) images. Here we obtain a clear image of the polymer nanowires using a super-resolution method (Fig. 8c). The well-defined polymer nanowires are shown in the SEM image (Fig. 8d). The distribution of diameters of the nanowires from the SEM images and super-resolution images are summarized in Fig. 8e by randomly selecting 50 different nanowires (Nano Measure 1.2). The diameters of the nanowires are obtained as ~150 nm from the images of SEM (Fig. 8e black column). The diameters of the nanowires calculated from the super-resolution images in the same way are slightly larger, which is averaged to ~170 nm (see Fig. 8e red column). By magnifying the green box area in Fig. 8c, the images of these nanowires are still clear and are identical.

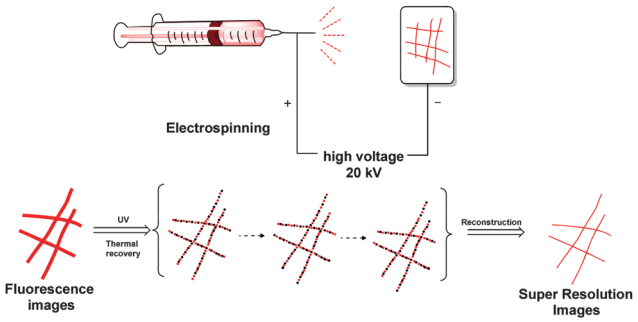

Scheme 2 A schematic drawing of electrospinning and the super-resolution imaging processes of the prepared nanowires.

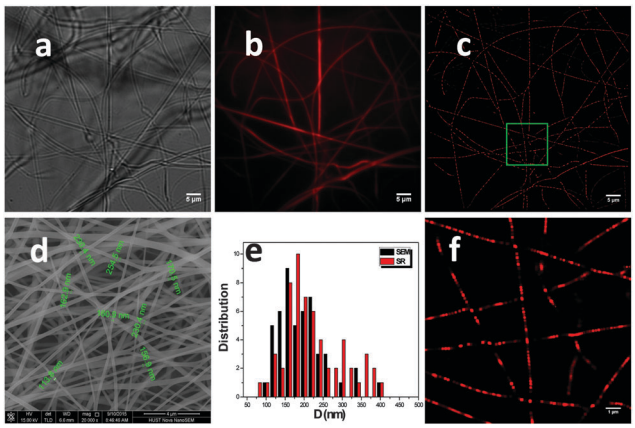

Fig. 8 Nanowires of PVP mixed with PMI–N–HABI prepared by electrospinning onto glasses. (a) Wide field image. (b) Fluorescence image. (c) Super-resolution image. (d) SEM image. (e) The distribution diagram of the diameters of the nanowires from SEM (black column) and super-resolution imaging (red column). (f) Enlarged area of the green box in (c); the electrospinning method: 1.0 g of PVP polymer (M_n = 1 300 000) was dissolved in ethanol (2.0 g) and DMF (7.0 g); to this solution 5.0 mg PMI–N–HABI was dissolved in darkness and then used for nanowire preparation directly.

Although the quality of super-resolution images is slightly inferior to that of SEM, the liquid-compatible imaging procedure without the necessity for high vacuum and high voltage will become a powerful optical nanovisualization tool, leading to the development of flexible photoswitchable fluorescent probes.

Conclusion

In conclusion, we report the design and synthesis of a fluorescence molecular switch, PMI–N–HABI, which possesses near-infrared emission, high fluorescence quantum yield, high switching ratio, fast photobleaching and fast spontaneous recovery of fluorescence. The emission of PMI–N–HABI is highly dependent on the polarity of the solvent, which is due to the ICT characters of "D–π–A" structures. In moderate polarity solvent DCM, PMI–N–HABI emits strong NIR light (715 nm) with fluorescence quantum yield as high as 0.29. Based on our former molecular design, the decoloration speeds of the two imidazyl radicals in PMI–N–HABI are strongly enhanced to 1.3 s at room temperature in toluene. The fast spontaneous recovery of fluorescence is attributed to the inhibited diffusion of the intramolecular photo-induced twin radicals. The fluorescence of PMI–N–HABIs i quenched under UV irradiation by a FRET process from the PMI moiety to the two radicals and the fluorescence recovers by the recombination of the two radicals. The fatigue resistance of PMI–N–HABI in solution could be repeated more than 100 times without clear photobleaching. We applied this probe into super-resolution imaging of nanowires prepared by electrospinning. The super-resolution images provide comparable quality with those of SEM images in a fast and convenient way. This novel photoswitching mechanism of near-infrared fluorophores will be promising as an exploratory optical nanoimaging tool controlled by a single wavelength laser for nanoscale optical visualization of living and non-living dynamic processes.

Author contributions

The manuscript was written through contributions from all authors. All authors have given approval for the final version of the manuscript.

Conflict and interest

The authors declare no competing financial interest.

Acknowledgements

This work was supported by the National Basic Research Program of China (Grant No. 2015CB755602 and 2013CB922104) and NSFC (21474034 and 21174045). We also thank the Analytical and Testing Center of Huazhong University of Science and Technology and the Center of Micro-Fabrication and Characterization (CMFC) of WNLO for the use of their facilities.

References

1 M. Irie, T. Fukaminato, K. Matsuda and S. Kobatake, *Chem. Rev.*, 2014, **114**, 12174–12277.
2 A. A. Beharry and A. D. Woolley, *Chem. Soc. Rev.*, 2011, **40**, 4422–4437.
3 R. Klajn, *Chem. Soc. Rev.*, 2014, **43**, 148–184.
4 S. Kawata and Y. Kawata, *Chem. Rev.*, 2000, **100**, 1777–1788.
5 (*a*) M. Natali and S. Giordani, *Chem. Soc. Rev.*, 2012, **41**, 4010–4029; (*b*) J. Andreasson and U. Pischel, *Chem. Soc. Rev.*, 2015, **44**, 1053–1069; (*c*) K. Li, Y. Xiang, X. Wang, J. Li, R. Hu, A. Tong and B. Z. Tang, *J. Am. Chem. Soc.*, 2014, **136**, 1643–1649; (*d*) J.-Y. Wu, C.-H. Yu, J.-J. Wen, C.-L. Chang and M.-K. Leung, *Anal. Chem.*, 2016, **88**, 1195–1201.
6 C. M. Sousa, J. Berthet, S. Delbaere, A. Polonia and P. J. Coelho, *J. Org. Chem.*, 2015, **80**, 12177–12181.
7 P. Zacharias, M. C. Gather, A. Köhnen, N. Rehmann and K. Meerholz, *Angew. Chem., Int. Ed.*, 2009, **48**, 4038–4041.

8 (*a*) M. Bates, B. Huang, G. T. Dempsey and X. Zhuang, *Science*, 2007, **317**, 1749–1753; (*b*) S. A. Jones, S. H. Shim, J. He and X. Zhuang, *Nat. Methods*, 2011, **8**, 499–508; (*c*) S. Manley, J. M. Gillete, J. H. Patterson, H. Shroff, H. F. Hess, E. Betzig and J. Lippincott-Schwartz, *Nat. Methods*, 2008, **5**, 155–157.

9 (*a*) H. Chen, N. Cheng, W. Ma, M. Li, S. Hu, L. Gu, S. Meng and X. Guo, *ACS Nano*, 2016, **10**, 436–445; (*b*) P. Lutsyk, K. Janus, J. Sworakowski, G. Generali, R. Capelli and M. Muccini, *J. Phys. Chem. C*, 2011, **115**, 3106–3114.

10 (*a*) Y. Wu, Y. Xie, Q. Zhang, H. Tian, W. Zhu and A. D. Q. Li, *Angew. Chem., Int. Ed.*, 2014, **53**, 2090–2094; (*b*) W. Li, X. Li, Y. Xie, Y. Wu, M. Li, X.-Y. Wu, W.-H. Zhu and H. Tian, *Sci. Rep.*, 2015, **5**, 9186.

11 H. Zhao, S. Sen, T. Udayabhaskararao, M. Sawczyk, K. Kučanda, D. Manna, P. K. Kundu, J.-W. Lee, P. Král and R. Klajn, *Nat. Nanotechnol.*, 2016, **11**, 82–88.

12 R. F. Khairutdinov and J. K. Hurst, *Langmuir*, 2004, **20**, 1781–1785.

13 (*a*) M. J. Rust, M. Bates and X. Zhuang, *Nat. Methods*, 2006, **3**, 793–795; (*b*) H. Shroff, C. G. Galbraith, J. A. Galbraith and E. Betzig, *Nat. Methods*, 2008, **5**, 417–423.

14 T. A. Golovkova, D. V. Kozlov and D. C. Neckers, *J. Org. Chem.*, 2005, **70**, 5545–5549.

15 Y. Zhang, K. Zhang, J. Wang, Z. Tian and D. Q. A. Li, *Nanoscale*, 2015, **7**, 19342–19357.

16 (*a*) M. Q. Zhu, L. Zhu, J. J. Han, W. Wu, J. K. Hurst and A. D. Q. Li, *J. Am. Chem. Soc.*, 2006, **128**, 4303–4309; (*b*) M. Q. Zhu, G. F. Zhang, C. Li, M. P. Aldred, E. Chang, R. A. Drezek and A. D. Q. Li, *J. Am. Chem. Soc.*, 2011, **133**, 365–372; (*c*) M. Q. Zhu, G. F. Zhang, Z. Hu, M. P. Aldred, C. Li, W. L. Gong, T. Chen, Z. L. Huang and S. Liu, *Macromolecules*, 2014, **47**, 1543–1552.

17 (*a*) C. Li and H. Wonneberger, *Adv. Mater.*, 2012, **24**, 613–636; (*b*) L. Chen, C. Li and K. Mullen, *J. Mater. Chem. C*, 2014, **2**, 1938–1956; (*c*) Y. Zagranyarski, L. Chen, Y. Zhao, H. Wonneberger, C. Li and K. Mullen, *Org. Lett.*, 2012, **14**, 5444–5447.

18 T. Fukaminato, T. Doi, N. Tamaoki, K. Okuno, Y. Ishibashi, H. Miyasaka and M. Irie, *J. Am. Chem. Soc.*, 2011, **133**, 4984–4990.

19 M. Berberich, A.-M. Krause, M. Orlandi, F. Scandola and F. Wurthner, *Angew. Chem., Int. Ed.*, 2008, **47**, 6616–6619.

20 X. Guo, D. Zhang and D. Zhu, *Adv. Mater.*, 2004, **16**, 125–129.

21 K. Mullen, *ACS Nano*, 2014, **8**, 6531–6541.

22 A. Keerthi, Y. Liu, Q. Wang and S. Valiyaveettil, *Chem. – Eur. J.*, 2012, **18**, 11669–11676.

23 T. Yamaguchi, Y. Kobayashi and J. Abe, *J. Am. Chem. Soc.*, 2015, **138**, 906–913.

24 S. Hatano, T. Horino, A. Tokita, T. OShima and J. Abe, *J. Am. Chem. Soc.*, 2013, **135**, 3164–3172.

25 K. Shima, K. Mutoh, Y. Kobayashi and J. Abe, *J. Am. Chem. Soc.*, 2014, **136**, 3796–3799.

26 H. Yamashita, T. Ikezawa, Y. Kobayashi and J. Abe, *J. Am. Chem. Soc.*, 2015, **137**, 4952–4955.

27 T. Ikezawa, K. Mutoh, Y. Kobayashi and A. Jiro, *Chem. Commun.*, 2016, **52**, 2465–2468.

28 H. Yamashita and J. Abe, *Chem. Commun.*, 2014, **50**, 8468–8471.

29 L. Feiler, H. Langhals and K. Polborn, *Liebigs Ann.*, 1995, 1229–1244.

30 D. Aigner, S. M. Borisov, P. Petritsch and I. Klimant, *Chem. Commun.*, 2013, **49**, 2139–2141.

31 M. Luo and K. Chen, *Dyes Pigm.*, 2013, **99**, 456–464.

32 C. Li, J. Schçneboom, Z. Liu, N. G. Pschirer, P. Erk, A. Herrmann and K. Mullen, *Chem. – Eur. J.*, 2009, **15**, 878–884.

33 R. Turrisi, A. Sanguineti, M. Sassi, B. Savoie, A. Takai, G. E. Patriarca, M. M. Salamone, R. Ruffo, G. Vaccaro, F. Meinardi, T. J. Marks, A. Facchetti and L. Beverina, *J. Mater. Chem. A*, 2015, **3**, 8045–8054.

34 F. Rodler, B. Schade, C. M. Jager, S. Backes, F. Hampel and C. Bottcher, *J. Am. Chem. Soc.*, 2015, **137**, 3308–3317.

35 Z. Chen, B. Fimmel and F. Würthner, *Org. Biomol. Chem.*, 2012, **10**, 5845–5855.

36 K. A. Kistler, C. M. Pochas, H. Yamagata, S. Matsika and F. C. Spano, *J. Phys. Chem. B*, 2012, **116**, 77–86.

37 C. Hippius, I. H. M. van Stokkum, E. Zangrando, R. M. Williams, M. Wykes, D. Beljonne and F. Würthner, *J. Phys. Chem. C*, 2008, **112**, 14626–14638.

38 W.-L. Gong, G.-F. Zhang, C. Li, M. P. Aldred and M.-Q. Zhu, *RSC Adv.*, 2013, **3**, 9167–9170.

39 W.-L. Gong, Z.-J. Xiong, C. Li and M.-Q. Zhu, *RSC Adv.*, 2014, **4**, 64371–64378.

40 W.-L. Gong, J. Yan, L.-X. Zhao, Z.-J. Xiong, C. Li, Z.-L. Huang and M.-Q. Zhu, Blue-Light-Induced Fluorescence Quenching and Spontaneous Recovery Enabling Single-Wavelength Controlled Optical Nanoimaging, in submitting.

